ELSEVIER

Catalysis Today 76 (2002) 121–131

CATALYSIS TODAY

www.elsevier.com/locate/cattod

Catalytic and photocatalytic ozonation of phenol on MnO_2 supported catalysts

Jorge Villaseñor [a,*], Patricio Reyes [b], Gina Pecchi [b]

[a] *Instituto de Química de Recursos Naturales, Universidad de Talca, Casilla 747, Talca, Chile*

[b] *Departamento de Físico-Química, Facultad de Ciencias Químicas, Universidad de Concepción, Casilla 160-C, Concepción, Chile*

Abstract

Different series of manganese-supported catalysts containing 10 wt.% of manganese, as oxide, on TiO_2 have been prepared by the sol–gel method and by the traditional method based on the impregnation of the support with the metal precursor on commercial and sol–gel supports. The samples were characterized by measuring the specific area (S_{BET}), temperature-programmed desorption (TPD), Fourier transform infrared (FTIR) spectroscopy, temperature-programmed reduction (TPR), electrophoretic migration (IP) and X-ray diffraction (XRD). The catalytic and photocatalytic activity was measured in a batch reactor using ozone as the oxidizing agent. The catalytic behavior, expressed as constant rate, in absence of irradiation did not show significant changes for the manganese-supported catalysts. The only exception was the cogelated Mn/TiO_2 catalyst, which showed higher degradation activity, the main product being benzoquinone. On the other hand, all the irradiated systems showed an increase in the phenol degradation, being CO_2 and small organic acids the final product.

Keywords: Photocatalysis; Phenol; Manganese; Titania; Sol–gel

1. Introduction

The most used and economic alternative of wastewater treatment is based on biological methods. However, industrial wastewater in many cases contains the biorecalcitrant chemical species that resist biological treatments. The biological treatments depend on many factors including pH, temperature, organic charge measured as biological demand of oxygen (DBO) and the presence of the inhibitors such as phenol species [1–3]. The concentration of these chemical compounds is usually below 1 ppm in seawater and half in river water without dilution capacity. This is in agreement with the regulation dealing with the evolution of phenolic compounds to the environment, regulated by different governmental agencies [4].

Phenolic compounds constitute a group of chemicals found in many industrial waste water processes such as pulp mills, manufacture of pesticides, dyes, tomato transformation processes, wine distilleries, olive oil productions and others [5–8].

Chemical oxidation such as ozone, ozone with UV, ozone with hydrogen peroxide, Fenton's reagents, and catalytic wet oxidation and physical adsorption on activated carbons are alternatives for the elimination of recalcitrant chemicals present in wastewater. In spite of the fact that chemical oxidation reactions can be more expensive than the other procedures, they have the advantage that they can eliminate the pollutants, whereas in the others they are removed from the effluents but not degraded. In catalytic oxidation processes, ozone can be used as an oxidant agent capable of degrading the phenolic species. However, this alternative can be expensive due to the

* Corresponding author.

0920-5861/02/$ – see front matter
PII: S0920-5861(02)00212-2

cost of production of ozone, generated in situ, and also because of the low solubility of ozone in aqueous solutions. The use of combined UV radiation and ozone is an attractive route because of the enhancement of the performance for both agents by means of the hydroxyl radical generation, a powerful oxidant agent that can oxidize completely the organic matter present in aqueous systems [9–12].

Under UV irradiation ($\lambda < 300$ nm) the hydroxyl radical ($OH^{\bullet}$) can be formed from photodissociation of H_2O_2 generated by ozone interaction with water [13]

$$O_3 + H_2O + h\nu \rightarrow H_2O_2 + O_2 \quad (1)$$

$$H_2O_2 + h\nu \rightarrow 2OH^{\bullet} \quad (2)$$

Irradiation over 300 nm lead to a reaction between ozone and H_2O_2 to produce hydroxyl radicals

$$O_3 + H_2O_2 \rightarrow OH^{\bullet} + HO_2^{\bullet} + O_2 \quad (3)$$

Several authors have mentioned that iron salts enhance the activity of ozone by an increase in the concentration of OH radicals. The role of iron has been related to the formation of FeO^{2+} species which can produce OH radicals from water, as mentioned by Ruppert and Bauer [14] and Sauleda and Brillas [15].

$$Fe^{2+} + O_3 \rightarrow FeO^{2+} + O_2$$

$$FeO^{2+} + H_2O \rightarrow Fe^{3+} + OH^{\bullet} + OH^{-}$$

The Mn(II) has been used as catalyst in the ozonation of same pollutants as atrazine, simazine and oxalic acid [16–18]. The role of Mn(II) in the oxalic acid at pH 4 is to interact with ozone to generate Mn(III) or Mn(IV) simultaneously with OH radicals which can also act as oxidant agents. Manganese dioxide has been used by Andreozzi et al. [19] in the oxalic acid ozonation. The authors proposed an interaction between oxalic acid and the surface of Mn(III) species leading to Mn(II) and CO_2. The role of ozone is to reoxidize the Mn(II) to Mn(III, IV). The influence of pH and temperature were studied and a better performance at low pH and high temperature (10–35 °C) was found. In spite of the promising results using manganese dioxide as a catalyst, only few studies have been published, and therefore, more detailed studies are required.

The aim of the present work is to study the performance of manganese dioxide supported on titania, as catalysts for the phenol photodegradation using ozone as the oxidant agent. This agent can avoid environmentally unfriendly chlorination treatments [20]. UV application enhances the activity of ozone, and the presence of a semiconductor as TiO_2 can provide an alternative route for phenol degradation. Correlation between catalytic and photocatalytic behaviors and surface and adsorption properties of manganese-supported catalysts prepared by impregnation and the sol–gel method were studied. The catalysts were characterized by nitrogen adsorption isotherm at 77 K, FTIR spectroscopy, UV-Vis absorbance, temperature-programmed reduction (TPR), temperature-programmed desorption (TPD) and X-ray diffraction (XRD). The degradation of phenol at 298 K in aqueous catalyst suspension was used as a test reaction.

2. Experimental

A commercial TiO_2-DegussaP25 and a TiO_2-SG (obtained by gelation of titanium Ti(IV) isopropoxide with *sec*-butanol at 343 K) were used as support of catalysts. The catalysts were prepared by impregnation, at 308 K, of a $Mn(NO_3)_2$ solution on the supports. Also, a cogelated catalyst, prepared by the cogelation of the manganese and the titania precursors, was prepared. MnO_2 loading was 10 wt.% in all the prepared catalysts. Titania sol–gel was prepared in one step in a reflux system at a constant temperature of 333 K using a water/solvent ratio of 4 in the gelation solution. The solids were dried at 393 K for 12 h and calcined in air at 773 K for 4 h. The solids were labeled as: $Mn(I)/TiO_2$-D and $Mn(I)/TiO_2$-SG for the catalysts prepared by impregnation on the titania support. The cogelated catalyst was labeled as Mn/TiO_2-CG.

Specific area and porosity were evaluated in an automatic Micromeritics system Model Gemini 2370, from N_2 adsorption isotherm at 77 K in the relative pressure range 0.05–0.995. TPR experiments were carried out in a TPR/TPD 2900 Micromeritics system provided with a thermal conductivity detector. The reducing gas was a mixture of 5% H_2/Ar (40 $cm^3\,min^{-1}$) and a heating rate of 10 $K\,min^{-1}$ was employed. TPD of ammonia was carried out using 50 $cm^3\,min^{-1}$ of Ar as carrier gas. Ammonia pulses were dosed in order to saturate catalyst surface at 373 K; then the

sample was cooled down to room temperature and once the base line was restored the temperature was linearly increased (10 K min^{-1}) up to 773 K. The IR spectra was recorded in a Magna-IR Nicolet 550. The isoelectric point (IP) was obtained by measuring the zeta-potentials as function of pH suspensions [21]. The measurements were carried out in a Zeta-Meter Inc. (Model ZM-77) using 20 mg of 2 μm catalyst particles ultrasonically suspended in 200 ml of 10^{-3} M KCl solution. XRD patterns were recorded in a Rigaku 3770 diffractometer using a Ni filter and Cu $K\alpha_1$ radiation, and Si as internal standard. Intensity was measured by step scanning in the 2θ range first between 3° and 70° at 1° min^{-1} and then the region between 20° and 50° was rescanned at 0.25° min^{-1}. Percent composition calculations were obtained by using the equation % rutile $= (1/((0.884\,A/R)+1)) \times 100$, A and R being the areas of anatase and rutile peaks, respectively, and 0.884 a scattering coefficient [22].

Catalytic activity measurements in the photodegradation of phenol were carried out at atmospheric pressure in a 150 cm^3 Pyrex glass batch reactor [23] with 100 cm^3 of aqueous solution containing 100 ppm of phenol and 1.500 g of powdered catalyst at a constant stirring rate (450 rpm), conditions in which no diffusional limitation is present (Weisz number $\leq$0.3) [24]. The external chamber of the reactor was kept at 298 K by circulation of water. The ozone, generated by an OZOCAV Laboratory Ozone Generator, was added to the reactor by a glass fibber filter placed at the bottom of the reactor. The reactor was placed in a black box during the reaction and the gas flow was kept constant at 50 cm^3 min^{-1}, having an ozone concentration of 2.15 mg/l. The analyses of the evolved CO_2 as a function of the reaction time were carried out by gas chromatography using a Shimadzu GC 8A provided with a Porapak Q column and thermal conductivity detector. The amount of evolved CO_2 provides a direct measurement of total phenol mineralization. The samples were irradiated through a quartz window placed in the top of the reactor with a General Electric UV mercury lamp (HR 250 DX 37/40). The lamp bandwidth is in the range 220–380 nm. The radiation intensity was measured from UVX-digital radiometer (UVP-INC) using a 254 and 365 nm sensor. The radiation intensity was measured behind the reactor quartz window and 15 cm from the lamp. At 254 and 365 nm the intensities were 1700 and 3700 μW/cm^2, respectively. Phenol was monitored by HPLC chromatography using a Perkin Elmer 200 Series GC provided with an autosampler and UV-Vis detector, and a column Lichrocart 250 RP18. The system was operated isocratically with a mixture of acetonitrile/phosphate buffer pH 3 (10:90, v/v), and the reaction was studied during 3 h. In all the experiments, the solid was removed from the solution prior analysis by filtration on a 20 μm membrane filter. The principal detected products, by HPLC, were: catechol (C), resorcinol (R), hydroquinone (HQ), 1,4-benzoquinone (BQ), 1,2-benzoquinone (OBQ), pyrogallol (PG), phloroglucinol (FG), hydroxyhydroquinone (HHQ), pyruvic acid (PA), maleic acid (MA), CO_2 and water.

3. Results and discussion

3.1. Specific area

The specific area and average pore radius obtained from nitrogen adsorption isotherms are compiled in Table 1. No significant changes in specific area were observed and the values fall in the range 40–140 m^2 g^{-1}. TiO_2 systems exhibit moderate surface area in the range 31–49 m^2 g^{-1}. A slight decrease in the surface area is observed upon the impregnation of the titania with manganese nitrate. Conversely, in the Mn/TiO_2 prepared by cogelation procedure, a significant increase in the surface area occurs without a decrease in the porous radii, indicating no access limitation to the porosity structure. The high surface area of the cogelated samples is attributed to the fact that manganese ions provide additional nucleation sites which lead to a solid with higher surface area [22].

Table 1
Specific surface area, average pore radius (Φ) and surface acidity of the studied catalysts

Catalyst	S_{BET} (m^2 g^{-1})	Φ (nm)	Surface acidity	
			meq g^{-1}	μmol m^{-2}
TiO_2-D	49	3.3	0.024	0.489
TiO_2-SG	38	3.0	0.030	0.789
Mn(I)/TiO_2-D	43	5.0	0.037	0.866
Mn(I)/TiO_2-SG	30	3.0	0.029	0.958
Mn/TiO_2-CG	138	3.0	0.070	0.505
MnO_2-bulk	1	10	0.095	0.298

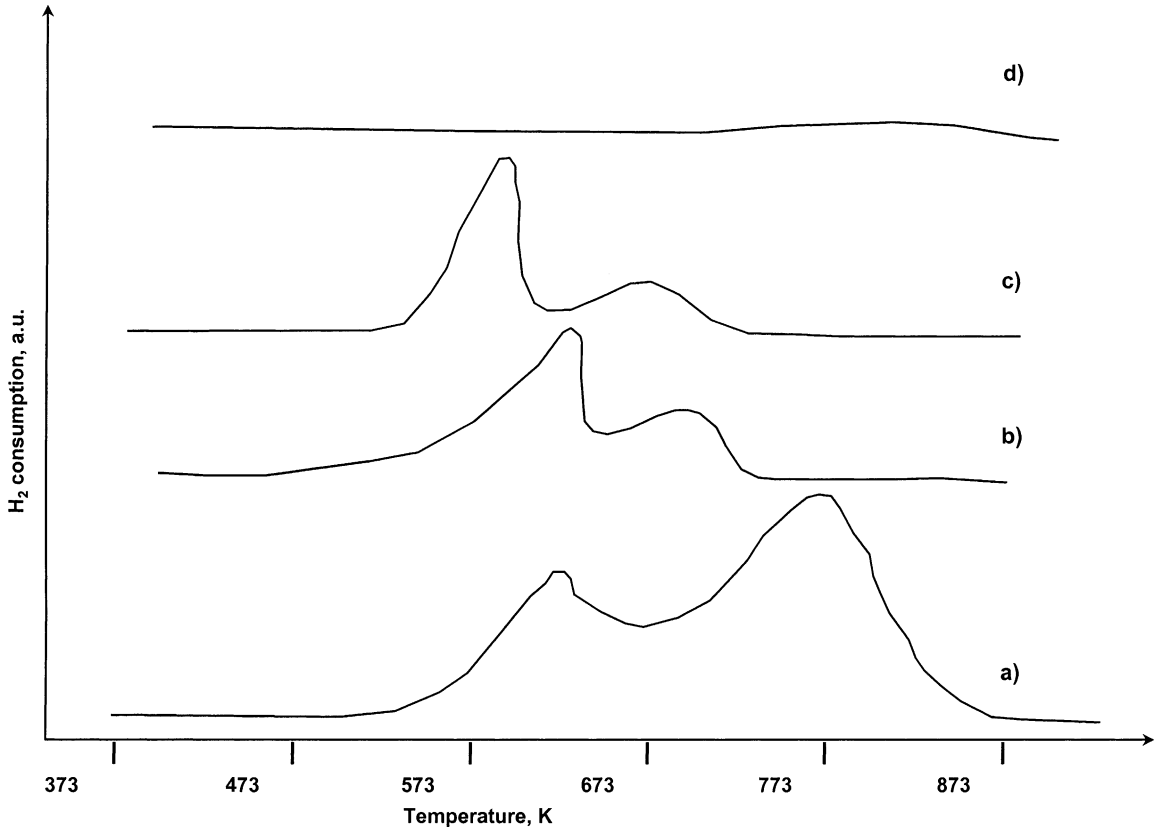

Fig. 1. TPR profiles for MnO_2 and MnO_2/TiO_2 catalysts: (a) MnO_2-bulk, (b) Mn(I)/TiO_2-D, (c) Mn(I)/TiO_2-SG, (d) Mn/TiO_2-CG.

3.2. TPR

No significant reduction for TiO_2 was observed in the studied temperature range from room temperature up to 1000 K (Fig. 1). On the other hand, bulk manganese oxide exhibits only two reduction peaks centered at 620 and 760 K. In the impregnated samples, two peaks centered approximately at 600 and 670 K were detected, suggesting the presence of two different manganese oxide species. The first at lower temperature, ca. 600 K, exhibits the highest intensity, whereas the second, at 670 K, possesses approximately one-third of the total hydrogenation consumption. The sample obtained by cogelation shows a low intensity broad single peak centered at about 800 K. This implies a low extent of reduction of manganese species in this catalyst, similar to the results reported by Mahoney et al. [25]. They found that reduction of manganese was not detectable up to 1000 K for MnO_2 supported on zeolites.

Impregnated catalysts showed comparable extent of reduction but lower than the stoichiometric. The reduction stoichiometry considered was $Mn^{4+} \rightarrow Mn^0$. Conversely, in the cogelated sample only a low fraction of the manganese oxide species are reduced which may be attributed to a partial insertion of manganese species into the TiO_2 lattice (Table 2).

3.3. TPD

The surface acidity was evaluated by TPD of ammonia. The TPD profile showed in all cases a single peak centered at about 500 K having differences in intensity according to the nature of the catalyst. The results were compiled in Table 1. MnO_2 possesses a higher specific acidity than TiO_2. On the other hand,

Table 2
Reduction temperature, extent of reduction expressed as mol H_2/mol MnO_2, IP and extent of anatase phase of the studied catalysts

Catalyst	T_{red} (K)	H_2/MnO_2 (mol%)	IP	Anatase (%)
TiO_2-D	–	–	6.1	83
TiO_2-SG	–	–	5.8	92
Mn(I)/TiO_2-D	614–678	70	5.6	81
Mn(I)/TiO_2-SG	576–666	72	5.3	100
Mn/TiO_2-CG	793	17	5.9	100
MnO_2-bulk	620–760	80	3.4	–

the specific surface acidity of the Mn/TiO_2 samples is higher than the one obtained by the support. This increment above the value observed for each of the pure oxide components could be due to the creation of additional interfacial acidic sites.

3.4. XRD

All the catalyst samples were studied by XRD. Fig. 2 displays the X-ray powder diffraction patterns of some representative samples. In the TiO_2-D and TiO_2-SG samples, the main diffraction lines correspond to rutile and anatase at $2\theta = 27.46^\circ$ and 25.35°, respectively, giving interplanar distances of 3.245 and 3.51 Å. Table 2 compiles the anatase extent in the prepared catalysts. The higher proportion of the anatase contribution in the TiO_2-SG is attributed to the high proportion of surface hydroxyl groups and to the insertion of metal ions in the titania lattice [26]. Thus, the Mn/TiO_2-cogelated catalyst showed only the anatase phase after calcination at 773 K. This is explained considering that during the synthesis process, manganese(II) ions can be located in octahedral positions substituent Ti species. Then, after the calcination treatment, when the lattice is already formed, Mn(II) ions remain inserted in such positions and the anatase structure remains stable. For the impregnated sample, the extent of anatase, as expected, is corresponds to the Degussa P-25 support.

Manganese oxide particle size was difficult to estimate from the X-ray line broadening, due to the fact that the most intense lines of the manganese oxide phases almost coincide with the diffraction lines of the support. Nevertheless, it was possible to detect the presence of MnO_2, by means of the MnO_2 line at $2\theta = 28.64^\circ$, which corresponds to an interplanar distance of 3.1143 Å. This line does not overlap

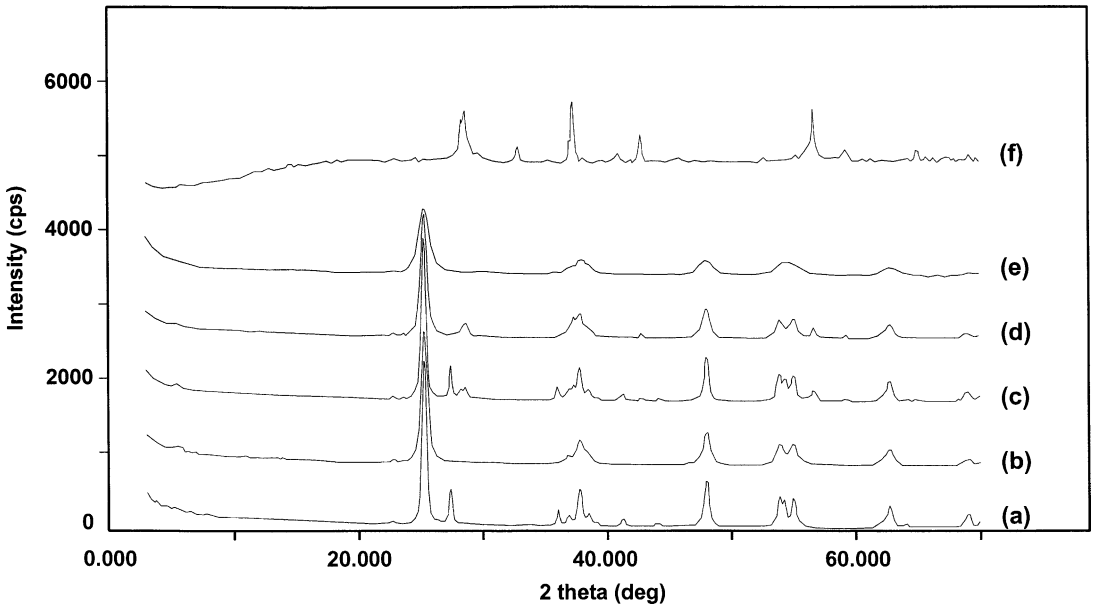

Fig. 2. XRD patterns: (a) TiO_2-D, (b) TiO_2-SG, (c) Mn(I)/TiO_2-D, (d) Mn(I)/TiO_2-SG, (e) Mn/TiO_2-CG, (f) MnO_2-bulk.

with any line of the titania; therefore, it can be used for this calculation. The line due to MnO_2 appears for the impregnated MnO_2/TiO_2 catalyst. This fact indicates that even though MnO_2 species are mainly dispersed on the support, a few particles of MnO_2 can be formed on the impregnated samples; therefore, MnO_2 exists in both states as patches of highly dispersed MnO_2 on TiO_2 and also as small crystals of this oxide. The X-ray powder diffraction of the Mn/TiO_2-cogelated catalyst does not exhibit any line in this region, indicating that the manganese oxide species remain highly dispersed and/or incorporated into the titania network. The cogelated sample exhibits only broad lines due to the support, characteristic of small particle size species and no lines due to manganese species were observed. Nevertheless, it is hard to believe that 10 wt.% of manganese deposited on a support having around 38 $m^2\,g^{-1}$ would exhibit high dispersion. Therefore, the possibility that Mn^{4+} may be partially incorporated to the titania network should be considered. This fact is likely, considering the similar ionic ratios and ionic charge of Mn^{2+}, Mn^{3+}, Mn^{4+} and Ti^{4+} (0.80, 0.66, 0.60 and 0.68 Å). Therefore, during the cogelation procedure, the Mn(IV) or Mn(III) can be located in the octahedral positions substituent Ti ions.

3.5. Electrophoretic migration

Electrophoretic migration measurements were carried out in order to evaluate the zero point charge (ZPC) of the studied solids. The measured IPs of all the studied solids are shown in Table 2. TiO_2 and MnO_2 exhibit IP of ca. 6.0 and 3.4, respectively. It is expected that upon the deposition of manganese oxide on the support, the ZPC may change from the value of the MnO_2 to higher ZPC values as a consequence of a surface coverage. As it can be seen in Table 2, the expected trend is observed and the obtained values allow to estimate from IP and ZPC values. These values show that ca. 20% of the support surface is covered by MnO_2 in both impregnated samples. For the cogelated sample, it is difficult to estimate the surface coverage due to the fact that the carrier is not a pure TiO_2 but it contains Mn inserted into the TiO_2 lattice; therefore, the reference IP is unknown.

3.6. Catalytic activity

Catalytic activity of the different samples was evaluated in the phenol oxidation either with ozone or with ozone plus UV radiation at 298 K. The detected degradation products are shown in Scheme 1. Some of these

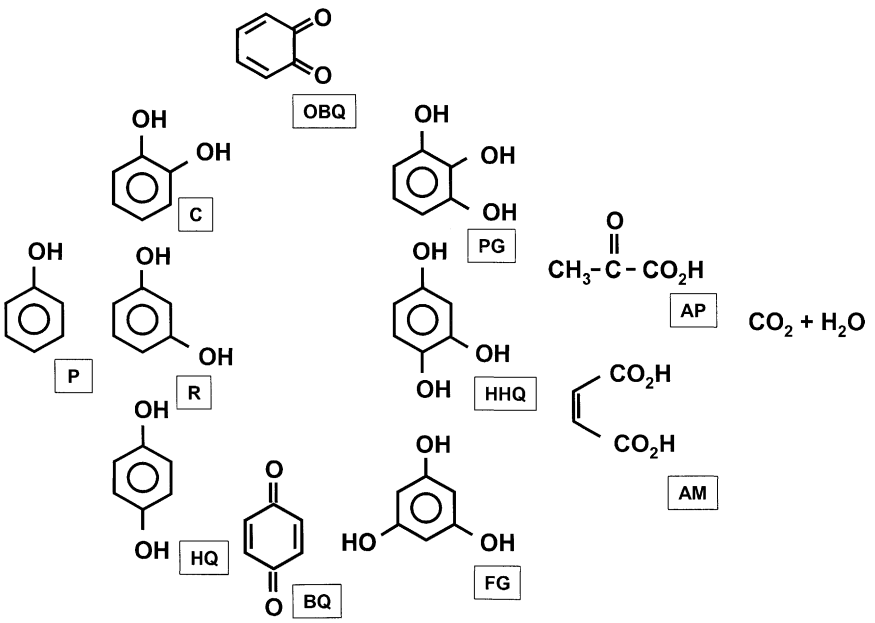

Scheme 1. Reaction pathway in the phenol degradation.

species, such as resorcinol (R), catechol (C) and hydroquinone (HQ), are likely primary oxidation products; the others are more oxidized species, and CO_2 and water, the final oxidation products. The mechanism depends on the nature of treatments, therefore, it is not likely that the mechanism and the constant value for the different oxidation steps may differ considerably. It should be mentioned that in absence of ozone and/or catalysts, the UV does not produce a significant degradation of the phenol.

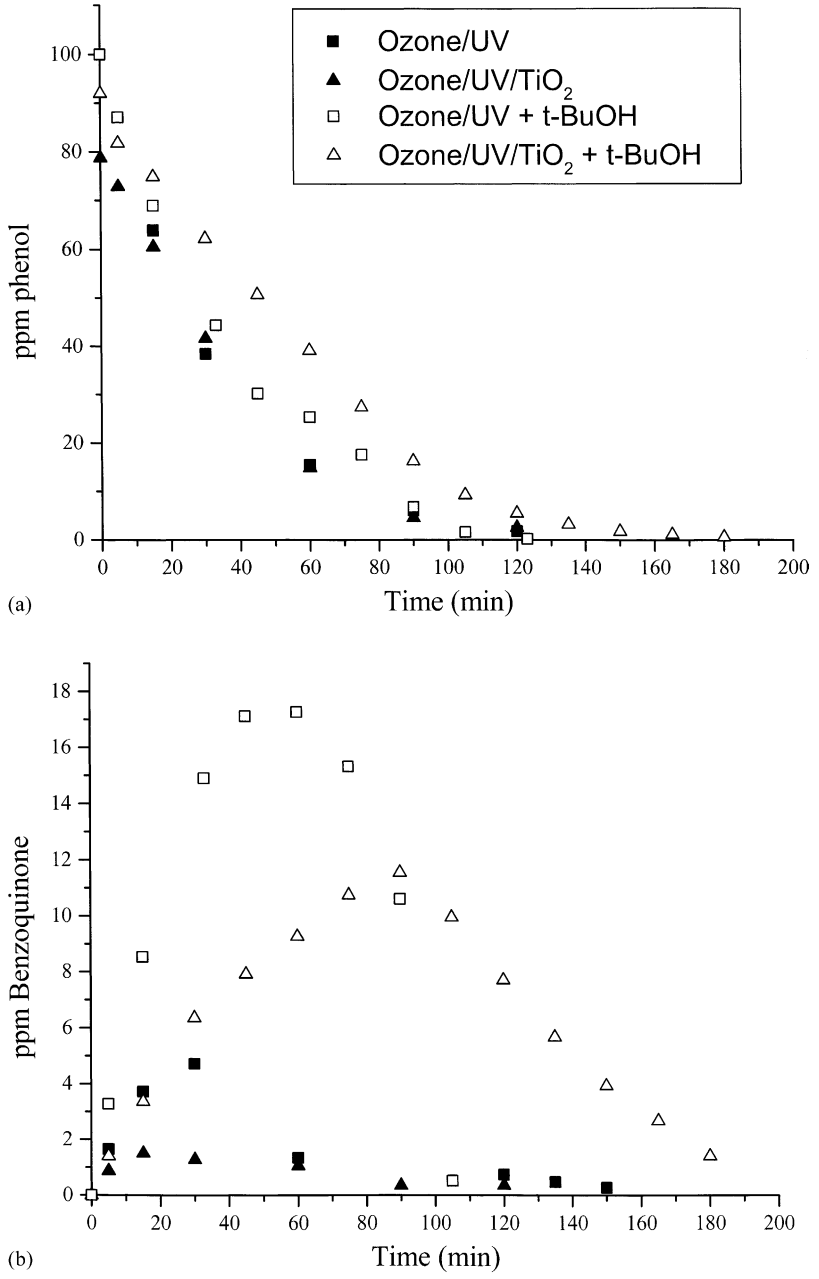

Fig. 3. (a) Phenol conversion and (b) BQ evolution.

Table 3
Phenol conversion (%P) with ozone at 298 K and extent of the main intermediates products in μmol/l at two different reaction times

System	%P[a]	%P[b]	C[a]	C[b]	R[a]	R[b]	HQ[a]	HQ[b]	BQ[a]	BQ[b]	PA[a]	PA[b]
Without catalyst	23.5	48.6	32.7	30.5	1.35	5.38	5.71	6.63	33.6	43.2	1.38	1.32
TiO_2-D	22.6	27.7	0	0	0.42	0	0	0.38	0.85	0.12	0	0
TiO_2-SG	10.1	13.0	0	0	0	0	0	0.20	0	0	0	0
Mn(I)/TiO_2-D	11.3	31.3	0.85	4.33	0	0	0	0	7.25	42.0	0.32	0.39
Mn(I)/TiO_2-SG	11.7	21.7	3.64	3.91	0.89	2.45	0	0.24	19.7	53.2	0.13	0.51
Mn/TiO_2-CG	26.0	64.7	9.63	9.5	4.7	16.5	8.28	12.9	65.6	137	2.47	3.40
MnO_2-bulk	13.6	46.3	10.2	14.9	0	0.41	0	1.88	36.3	91.4	0.95	4.63

[a] 40 min.
[b] 100 min.

Fig. 3a displays the evolution of phenol in time using different degradation systems such as ozone + UV, ozone + UV + TiO_2, ozone + UV + radical scavenger (*tert*-butyl alcohol, *t*-BuOH) and ozone + UV + TiO_2 + radical scavenger, and Fig. 3b displays the evolution of one of the main intermediates, BQ. As expected, in Fig. 3b the presence of this compound reaches a maximum and then decreases to an undetectable level. In Fig. 3a the presence of a scavenger not affecting the conversion level indicates that the action does not take place as a result of a radical mechanism. The phenol oxidation in the presence of ozone, UV and catalyst with *t*-BuOH is no evidence of the formation of hydroxyl radicals. Therefore, the adsorbed phenol is attacked directly by the ozone. On the other hand, in the oxidation with ozone, UV and catalysts, the presence of hydroxyl radicals—which contribute to the oxidation of the reaction intermediate—was detected. It can be clearly seen that in the presence of scavenger radicals, a maximum with much higher intensity can be reached. This demonstrates that the oxidation of the intermediates is produced essentially by radical species. Similar behavior was also observed in all the other intermediates which were also studied (data not shown for lack of space).

Tables 3 and 4 show that all the studied catalytic systems generated the same kind of intermediates with differences in their concentration, indicating that the reaction rates in the corresponding steps are different. The results may suggest that the *p*-hydroxylation of phenol generates HQ and is the first step followed by a fast oxidation to BQ. Under UV irradiation BQ is quickly oxidized to MA and CO_2.

Under ozone flow in the presence or absence of UV, low activities were displayed by all the prepared catalysts, showing experimental curves which can have an appropriate fit to pseudo-first-order reaction. The constant rates for catalyzed reactions were in the range 0.8×10^{-3} to 1.4×10^{-3} min^{-1}, shown in Table 5, with the only exception of the Mn/TiO_2-CG sample, whose activity is ca. 5 times higher. Significant differences in both the activity and the selectivity were found when the studies were performed in the presence of ozone and UV radiation. In fact, all the

Table 4
Phenol conversion (%P) with ozone and UV at 298 K and extent of the main intermediates products in μmol/l at two different reaction times

System	%P[a]	%P[b]	C[a]	C[b]	R[a]	R[b]	HQ[a]	HQ[b]	BQ[a]	BQ[b]	PA[a]	PA[b]
Without catalyst	31.3	74.1	1.59	6.25	3.31	22.6	0.92	0.75	8.93	27.1	5.37	13.2
TiO_2-D	37.1	67.2	0.59	0.28	3.43	10.4	2.53	3.46	1.32	0.62	19.7	18.1
TiO_2-SG	77.0	98.6	12.2	6.83	2.97	0	10.4	5.23	18.2	0	21.1	6.50
Mn(I)/TiO_2-D	69.2	91.0	0	0	0	4.82	24.7	1.76	17.2	10.1	0	0
Mn(I)/TiO_2-SG	60.5	92.9	14.0	2.81	10.5	10.7	1.23	0.80	125	112	27.4	42.6
Mn/TiO_2-CG	38.0	76.2	44.3	57.7	0.63	3.67	0.17	0.37	2.09	3.96	238	257
MnO_2-bulk	52.5	86.0	10.8	0.98	2.88	2.99	19.4	15.5	111	101	33.6	45.0

[a] 40 min.
[b] 100 min.

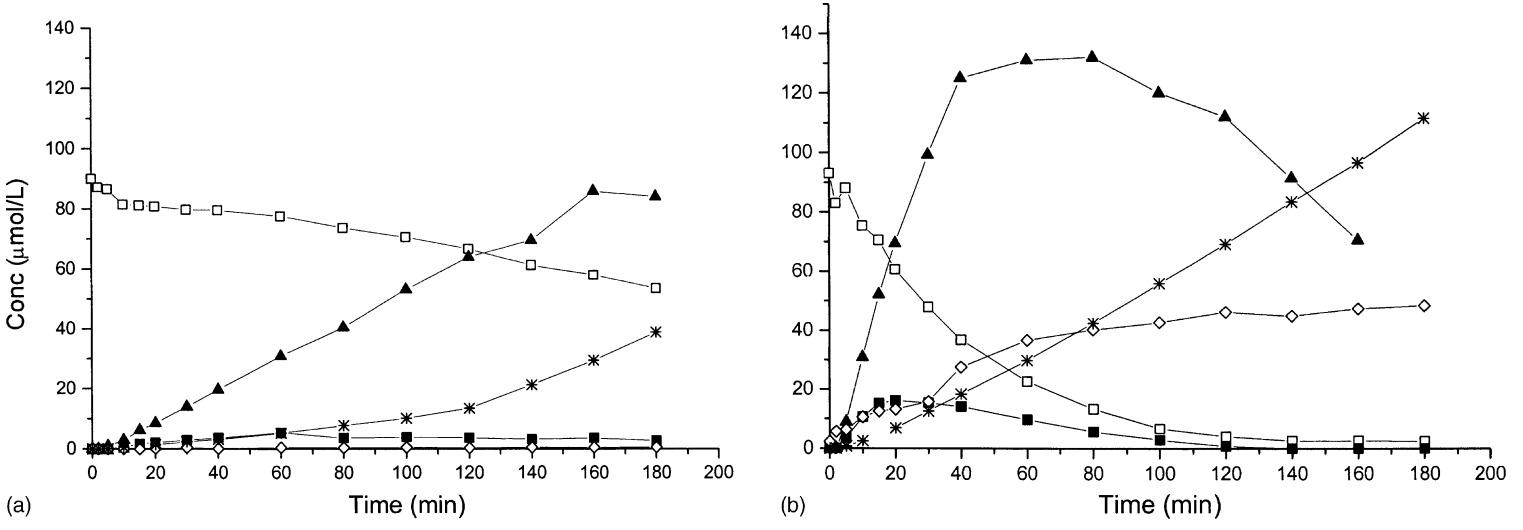

Fig. 4. Product distribution for Mn/TiO_2-CG: (a) without UV, (b) under UV irradiation. (□) P/10, (■) C, (▲) BQ, (◇) PA, (✳) CO_2.

Table 5
Pseudo-first-order constant, total conversion and yield of mineralizaton at 180 min of reaction in the degradation of phenol of the studied catalysts

System	$k \times 10^{-3}$ (min^{-1})		YM (%)	
	O_3	$O_3 + UV$	O_3	$O_3 + UV$
Without catalyst	3.1	4.1	4.3	6.2
TiO_2-D	1.1	4.7	5.5	31.2
TiO_2-SG	0.8	19	11.5	20.2
Mn(I)/TiO_2-D	1.4	13.7	6.8	17.6
Mn(I)/TiO_2-SG	1.0	11	6.1	17.5
Mn/TiO_2-cogelated	5.0	6.0	3.3	12.2
MnO_2-bulk	1.4	9.2	4.6	9.0

catalyzed systems showed significant enhancements in the activity, being the constant rate value in the following order: TiO_2-D < Mn/TiO_2-CG < MnO_2-bulk < Mn(I)/TiO_2-SG < Mn(I)/TiO_2-D < TiO_2-SG.

Table 5 summarizes the constant rate (k) of degradation of phenol at 298 K and pH = 4.5. The large differences observed in the activity due to the presence of UV can be explained in terms of hydrogen peroxide and hydroxyl radicals generation, as it has been mentioned previously [13]. In the manganese-supported on titania, either impregnated on TiO_2-D or TiO_2-SG, the catalytic activity is ca. 10 times higher than the values exhibited in absence of UV. As it was explained the additional OH radicals, which are powerful oxidants, can non-selectively attack the organic intermediates to complete mineralisation. It was observed that under UV irradiation the CO_2 production level is higher than the non-irradiated systems. On the other hand, the Mn/TiO_2-CG showed only moderate increases in the constant rate. This fact may be attributed to the insertion of manganese ions in the lattice of TiO_2, shifting the ability of the TiO_2 to produce hole and electrons, an important step in the pathway to produce the hydroxyl radicals. Besides the enhancement of the activity, the product distribution has also changed, as shown in Table 5. The yield of mineralisation (YM) obtained from the evolved CO_2 increases for all the samples approximately three times when the reaction is carried out in the presence of $O_3 + UV$ and catalysts, indicating a more effective oxidation. Additionally, the evolution of oxidation products such as BQ and AM, showed the typical curves for intermediate products that reach a maximum and then slope down. Obviously, the maximum of BQ appears at a lower time than AM as expected considering that AM is generated by oxidation of primary oxidized intermediates such as BQ.

The unusually high constant rate exhibited by TiO_2-SG in the presence of $O_3 + UV$ may be explained considering the high hydroxyl surface population of this sample. This high surface concentration, confirmed by the FTIR results, is supported by the fact that the large extent of the anatase phase (92%)—even though it was calcined at 773 K—was responsibility of the surface hydroxyl. This stabilization is due to the large size of the anatase channel that can easily accommodate the hydroxyl groups. The anchorage of manganese ions on the support take place on these hydroxyl groups, thus decreasing the hydroxyl population. This may explain the lower activity of the Mn(I)/TiO_2-SG.

In Fig. 4 the product distribution for non-irradiated and UV irradiated experiences can be observed for Mn/TiO_2-SG system. In the irradiated systems, more oxidized products than in the non-irradiated systems may be observed. Simultaneously, the high production of CO_2 was observed under UV irradiation as a consequence of the large amount of OH radicals generated in this situation, as was previously discussed.

4. Conclusions

Manganese/titania SG catalysts did not show any diffraction line attributed to manganese oxide species, indicating incorporation to the titania lattice and high dispersion of this phase.

Catalytic results indicate that the activity of the catalysts, in which manganese is incorporated to the titania network, is higher compared with the other counterparts. All the manganese-supported catalysts exhibit higher catalytic activity, regarding the weight of MnO_2, compared to the pure MnO_2. An enhancement in the catalytic activity in the irradiated systems was observed in most cases, except in the cogelated manganese–titanium dioxide. However, in this latter system, the irradiation did not significantly affect the activity. The product distribution is oriented to more oxidized products—pyruvic, maleic acids and CO_2—when the catalysts are irradiated with UV light. It was shown that phenol reacts directly with ozone but not with hydroxyl radicals as intermediates do.

Acknowledgements

The authors thank Prof. F. Javier Gil, from the Universidad de Santiago de Chile, for the electrophoretic migration measurement and CONICYT-CHILE (FONDECYT Grant 1000702) for the financial support.

References

[1] P. Pitter, Chudoba, Biodegradability of organic substances in the aquatic environment, CRC Press, Boston, 1990.
[2] A. Sarma, D. Kachroo, R. Kumar, Environ. Monitor. Assesm. 76 (2) (2002) 195.
[3] M. von Sperling, Principios basicos do tratamento de esgotos, vol. 2, Universidade Federal de Minas Gerais, 1996. ISBN 85-85266-05-8.
[4] Norma Chilena Oficial de Emisión de Contaminantes, NCh 2313/Of 98.
[5] R.L. Autenrieth, J.S. Bonner, J. Haz. Mater. 28 (1991) 29.
[6] J. Del Valle, A. Vázquez, Grasas Aceites 41 (1980) 309.
[7] A. Rambaud, J. Bontoux, Les effluents de conserveries de tomates, Bull. Bimestriel INACOL 25 (1974).
[8] F. López, J.L. Ovelleiro, Depuración de las aguas residuales de las destilerías de alcohol vínico, Ing. Quim. 109 (1978) 167.
[9] W.H. Glaze, G.R. Peyton, S. Lin, F.Y. Huang, J.L. Burlesson, Environ. Sci. Technol. 16 (1982) 454.
[10] P. Paton, J. Prado, A. Marco, E. Chamarro, S. Esplugas, in: 1st International Conference on Advanced Technologies for Water and Air Remediation. Use of Ozone and Ozone/UV for the Degradation of Pesticides, London, Canada, 1994.
[11] G.R. Peyton, W.H. Glaze, Environ. Sci. Technol. 22 (1988) 761.
[12] M. Legrini, E. Oliveros, A.M. Braun, Chem. Rev. 93 (1993) 671.
[13] G.R. Peyton, in: N.M. Ram, R.F. Christian, K.P. Canto (Eds.), Significance and Treatment of Volatile Organic Compounds in Water Supplies, Lewis Publishers, 1990, pp. 313–362.
[14] G. Ruppert, R. Bauer, Chemosphere 28 (1994) 1447.
[15] R. Sauleda, E. Brillas, Appl. Catal. B 29 (2001) 135.
[16] J. Ma, J.D. Graham, Ozone Sci. Eng. 19 (1997) 227.
[17] J. Rivas, E. Rodríguez, F. Beltrán, J. García-Araya, P. Alvarez, J. Environ. Sci. Health B 36 (3) (2001) 317.
[18] R. Andreozzi, A. Insola, V. Caprio, G.D. D'Amore, Wat. Res. 26 (7) (1992) 917.
[19] R. Andreozzi, A. Insola, V. Caprio, R. Marotta, V. Tufano, Appl. Catal. A 138 (1996) 75.
[20] H. Gallard, U. Von Gunten, Wat. Res. 36 (2002) 65.
[21] R.J. Hunter, Zeta Potential in Colloid Science, Principles and Applications, Academic Press, New York, 1981.
[22] X. Fu, W.A. Zeltner, Q. Yang, M.A. Anderson, J. Catal. 168 (1997) 482.
[23] G. Pecchi, P. Reyes, P. Sanhueza, J. Villaseñor, Chemosphere 43 (2001) 141.
[24] R.B. Bird, W.E. Stewart, E.N. Lightfoot (Eds.), Fenómenos de transporte, Editorial Reverte, 1975 (in Spanish).
[25] F. Mahoney, R. Rudham, J.V. Summers, J. Chem. Soc., Faraday Trans. I 75 (1979) 314.
[26] G. Pecchi, P. Reyes, T. López, R. Gómez, A. Moreno, J.L.G. Fierro, Effect of precursor on surface and catalytic properties of Fe/TiO_2 catalysts, J. Chem. Technol. Biotechnol. 77 (2002) 944.